Non-Oxidative Conversion of Methane with Continuous Hydrogen Removal

Richard W. Borry III (rborry@violet.berkeley.edu, 510-643-0930)
Enrique Iglesia (iglesia@cchem.berkeley.edu, 510-642-9673)

Department of Chemical Engineering
University of California at Berkeley
201 Gilman Hall
Berkeley, CA 94720

Materials Sciences Division
E. O. Lawrence Berkeley National Laboratory
1 Cyclotron Road
Berkeley, CA 94720

1. Introduction

Over the past fifteen years, studies of methane conversion have explored its oxidative coupling to C_2 hydrocarbons on metal oxides [1-3] and its non-oxidative conversion to aromatics on supported MoO_3 catalysts. [4-7] Unrestricted chain growth during endothermic methane pyrolysis reactions leads to the undesired formation of polynuclear aromatics and solid carbon. In addition, non-oxidative conversion of methane to benzene is limited by thermodynamics to a maximum yield of about 12% at 700°C. [7] Oxidative coupling of methane avoids thermodynamic limitations and pyrolytic chain growth by coupling C-H bond activation steps with the removal of surface hydrogen via oxidation with O_2. These reactions are, however, unselective and lead to high yields of undesired CO_2, limiting the yield of C_{2+} products to about 25% in conventional reactors. [3, 8]

2. Objectives

The objective of our research is to overcome the restrictions of non-oxidative methane pyrolysis and oxidative coupling of methane by transferring hydrogen across a selective inorganic membrane between methane and air streams, without the simultaneous transport of hydrocarbon reactants or products. This will make the overall reaction system exothermic, remove the thermodynamic barrier to high conversion, and eliminate the formation of carbon oxides.

Research sponsored by the U.S. Department of Energy's Federal Energy Technology Center, under contract DE-AC03-76SF00098 with the Morgantown Energy Technology Center, Morgantown, West Virginia 26505.

3. Approach

Our approach is to couple C-H bond activation and hydrogen removal steps by transporting hydrogen atoms through a dense ceramic membrane separating the methane and O_2 reactants. In our membrane reactor, catalytic methane pyrolysis produces C_{2+} hydrocarbons and aromatics on one side of the membrane and hydrogen is removed through an oxide film and combusted with air on the opposite side of the membrane. This process leads to a net reaction with the stoichiometry and thermodynamic properties of oxidative coupling, but without contact between the carbon atoms and oxygen species. Figure 1 shows the proposed configuration.

Figure 1: Methane conversion in a hydrogen-transport membrane reactor.

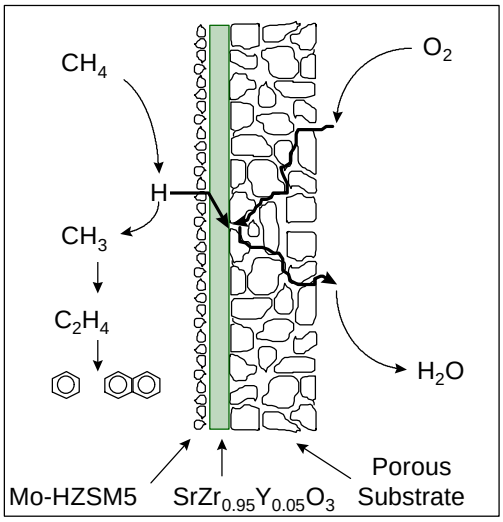

Our research program combines experimental and theoretical methods. First, we have developed a reaction-transport model of this system in order to identify intrinsic yield limitations and to predict optimum performance. This model includes detailed homogeneous reaction pathways for methane pyrolysis on the methane side and a set of surface reactions involved in the formation of alkyl radicals, the diffusion and recombination of H atoms, and the reactions of hydrocarbon products on surface sites. With this model, we can rigorously probe the effects of surface and gas-phase reactions, feed composition, hydrogen removal rate, temperature, and pressure.

Our experimental program attacks in parallel the design of methane pyrolysis catalysts and hydrogen transport thin film membranes. For catalytic methane pyrolysis, we report experimental results using the Mo/H-ZSM5 catalyst, which converts CH_4 to ethylene, benzene, toluene, and naphthalene with high selectivity and near-equilibrium conversion at 700°C. [4, 5, 7, 9] For selective hydrogen transport, we have used thick discs (1 mm thickness) of $SrZr_{0.95}Y_{0.05}O_3$ oxide, a known hydrogen conductor at temperatures from 200-900°C. [10, 11] Ongoing research using highly sinterable powders made using the glycine-nitrate process [12] attempts to form thin films (~10 μm thickness) of $SrZr_{0.95}Y_{0.05}O_3$ via spin-coating onto a porous NiO/CeO_2 ceramic support.

4. Project Description

4.1 Computer simulations

Based on oxidative coupling results, gas-phase reactions are expected to occur at the high temperatures normally required for methane activation under pyrolysis conditions. [8, 13] A kinetic model was constructed to accurately describe the rate and selectivity of homogeneous pyrolysis reactions of light alkanes in the temperature range 300 to 1000°C. The gas-phase reaction network contains 62 elementary reaction steps involving 35 species. This network was assembled by reduction of a larger set of hydrocarbon reactions extracted from literature compilations. [13-16] Rate parameters for some reactions involving high molecular weight species were estimated using the program CHEMACT to estimate rate constants as functions of temperature and pressure. [17, 18] All steps in the mechanism are assumed to be elementary, with reverse rate constants determined from thermodynamic equilibrium constants. Thermodynamic properties for all species were extracted from literature reports, when available [19], or calculated using group additivity methods. [20, 21]

In our simulations, we consider the production of aromatics larger than naphthalene ($C_{10}H_8$) to be undesired precursors to solid carbon (soot or coke) species. Therefore, all C_{11+} species are lumped into one group, designated as PNA (polynuclear aromatic hydrocarbons). [22] Overall, the concentrations of species C_1-C_{10} are determined by the detailed kinetic network, while those of the species C_{11+} are determined by a lumped PNA mechanism.

In oxidative coupling of methane, the catalyst serves as a methyl radical generator. [23-25] In order to probe the effect of such a catalyst on the methane pyrolysis system, we added the set of surface reactions below to the homogeneous reaction network:

$$CH_4 + [*] \xleftrightarrow{k_1} CH_3 \cdot + [H*] \quad (1)$$

$$2[H*] \xleftrightarrow{k_2} H_2 + 2[*] \quad (2)$$

In these equations, [*] and [H*] denote vacant and hydrogen-occupied surface sites, respectively. This set of reactions describes an “ideal” methyl radical generator, with a high hydrogen bond strength and weak carbon bond, so that the surface-carbon bond can be considered short-lived.

The role of a hydrogen transport membrane in a heterogeneous-homogeneous methane reaction system is to remove hydrogen from the system. Since hydrogen must first absorb on a surface before it dissolves into the membrane and undergoes solid-state diffusion, we simulate the entire H-removal process by a single irreversible reaction:

$$[H*] \xrightarrow{k_3} [*] \quad (3)$$

This equation assumes that the active site of hydrogen abstraction from methane is also the site of hydrogen dissolution into the membrane bulk. This situation would also be achieved in the case of separate methane activation and hydrogen removal sites when hydrogen dissolution into the membrane is quasi-equilibrated. The irreversible rate constant for this reaction can be estimated from the Fickian diffusion coefficient of the hydrogen-transport membrane and the film thickness. For two known hydrogen conductors, $SrCe_{1-x}Yb_xO_3$ and $SrZr_{1-x}Y(Yb)_xO_3$, (x = 0.01-0.1) [10, 26], this rate constant is predicted to vary from 10^{-4} cm/s for a 1 mm thick membrane at 700°C to 10^{-1} cm/s for a 0.01 mm thick membrane at 900°C.

We use the CHEMKIN II subroutine package and the DVODE ordinary differential equation solver [27] to simulate the behavior of our reaction network for the perfectly-stirred batch (or plug flow) reactor geometry. The SENKIN sensitivity subroutine package with the DASAC ordinary differential equation solver [28] was used to calculate sensitivity coefficients in order to identify the most important reaction pathways and to eliminate unimportant reactions and rate parameters. Complete details of the development of the computer model and reaction network are being reported elsewhere. [29]

4.2 Catalytic methane pyrolysis

Cation-exchanged zeolites based on Mo/H-ZSM5 compositions have been recently reported to form ethylene and benzene with high selectivity at 700°C, but thermodynamic constraints limit yields to about 10%. [7] For our catalytic experiments, H-ZSM5 was prepared by ion-exchange of ~10 g Na-ZSM5 (Zeochem, Si:Al = 14) with a 350 ml solution of 1.0 M NH_4NO_3 in deionized (DI) water at 60°C. The resulting NH_4-ZSM5 was separated by vacuum filtration and washed three times with DI water. The ion-exchange and wash process was repeated three additional times before the powder was dried overnight at 125°C. The dry powder was crushed lightly with a mortar and pestle and calcined at 500°C for 6 hours in flowing air (99.999%) to form H-ZSM5.

H-ZSM5 was physically mixed with MoO_3 (Johnson Matthey, 99.95% pure) using an alumina mortar and pestle to give a nominal Mo loading of 2.0% by weight. The mixture was calcined in flowing air at 500°C for 24 hours. After calcination, no MoO_3 peaks were detected by X-ray diffraction. Samples calcined at 475°C for 10 hours showed MoO_3 peaks in the XRD pattern, indicating incomplete dispersion of the MoO_3 crystallites throughout the zeolite. Elemental analysis by atomic absorption spectroscopy after final calcination gives the expected Mo content (2.12 wt%): therefore, there was no loss of MoO_3 by sublimation or migration onto the quartz boat. We interpret the disappearance of MoO_3 peaks in the XRD pattern as an indication of high dispersion of MoO_3 throughout the zeolite. Several other groups have reached similar conclusions [4, 5], and the low melting point of MoO_3 (795°C) [30] makes solid-state surface diffusion likely at 500°C. The calcined catalyst powder was pressed into pellets, crushed lightly, and sieved to 250-355 μm for further tests.

Catalyst reactor studies were conducted in a quartz cell with 6 mm diameter held isothermally within a temperature-controlled furnace. The catalyst loading was 1.0 g for isothermal studies and 0.1 g for temperature-programmed studies. The catalyst temperature was measured with a type K thermocouple placed inside a quartz thermowell in the center of the catalyst bed. All gases were of greater than 99.99% purity and were further purified by flowing through a molecular sieve (13X and 5A) trap before use. Flow rates were monitored and controlled using Porter mass flow controllers. Methane was supplied by Matheson as a 1:1 mixture in argon; Ar was used as an internal standard to measure accurately the amount of carbon remaining on the catalyst. Gas products were sampled on-line with a Sigma 2000 gas chromatograph (GC). Hydrocarbon products were separated with an HP-1 capillary column (Hewlett-Packard Inc.) and quantified using a flame ionization detector. Light gases (Ar, CO, CH_4, CO_2) were measured with a Carboxen 1000 packed column (Supelco, Inc.) and a thermal conductivity detector. Detection limits were about 1 ppm with the FID and 50 ppm with the TCD. For the temperature-programmed studies, products were measured with a shortened GC program, which allowed measurement of only CH_4, Ar, C_2's and aromatic products.

Powder X-ray diffraction (XRD) patterns were obtained using a Siemens Diffractometer D5000 with Cu K-α radiation (λ = 1.5406 Å), and analyzed using the DiffracAT software package. The scan rate was 0.010° per second, and crystal phases were assigned by comparison with the JPDS database.

Temperature-programmed reduction (TPR) studies with hydrogen were carried out on both bulk and supported MoO_3. Samples containing about 2 mg of molybdenum were loaded into a 6 mm (O.D.) tube. A mixture of 20% hydrogen in argon was passed over the sample at a flow rate of 80 ml/min, while heating from 25 to 1050°C at 10°C/min. This high flow rate was used in order to prevent depletion of hydrogen from the gas stream and to rapidly sweep away evolved water, which has an inhibitory effect on the reduction of supported MoO_3. [31] Water was removed from the cell's exit stream by absorption in a narrow bed of anhydrous $CaSO_4$ ("Drierite") before reaching the detector. Hydrogen consumption was measured by comparing the inlet and outlet streams with a thermal conductivity detector at 150 mA current.

4.3 Hydrogen-transport films

The oxides of $SrZr_{0.95}Y_{0.05}O_3$ and $SrCe_{0.95}Yb_{0.05}O_3$ composition with perovskite structures have been shown to selectively transport hydrogen at temperatures from 200-900°C. [10, 11, 32] Above ~900°C, these materials become mixed conductors, transporting both oxygen and hydrogen. Our studies focus on $SrZr_{0.95}Y_{0.05}O_3$, which we have found (in contradiction to reports in the literature [33]) to be more easily formed into dense, stable membrane discs and thin films. In addition, $SrZr_{0.95}Y_{0.05}O_3$ is less easily reduced than $SrCe_{0.95}Yb_{0.05}O_3$ in hydrogen atmospheres, and is less prone to form $SrCO_3$ in the presence of CO_2 at high temperatures. [34, 35]

$SrZr_{0.95}Y_{0.05}O_3$ is stable as an oxide at 500°C and below. [36] Above 500°C, irreversible reduction of the oxide phase occurs in reducing atmospheres. However, a small partial pressure of H_2O vapor (~3 kPa) prevents the reduction of $SrCe_{0.95}Yb_{0.05}O_3$ even in hydrogen atmospheres up to 900°C [37], and of $SrZr_{0.95}Y_{0.05}O_3$ above 500°C. Therefore, operation of a $SrZr_{0.95}Y_{0.05}O_3$ membrane for CH_4 pyrolysis will require either temperatures below 500°C or the presence of at least 3 kPa of H_2O vapor on the methane side.

Most of the experimental research using $SrZr_{0.95}Y_{0.05}O_3$ has involved its application in electrochemical fuel cells. The primary current carrier through $SrZr_{0.95}Y_{0.05}O_3$ has been shown to be protons below 500°C and electrons above 700°C. [10] Consequently, electrochemical cells attempting to drive hydrogen from one side to the other are only expected to work below 700°C, and will have high current efficiency only below 500°C. In dry air, below 500°C, the membrane will conduct hydrogen as protons, although the protonic concentration is less than half that in wet (3 kPa H_2O) atmosphere. [38]

The diffusion coefficient of H_2 through $SrZr_{0.95}Y_{0.05}O_3$ at 700°C (non-electrochemically driven) is 1.4 $x10^{-5}$ cm^2/sec. [11] The H-concentration in both $SrZr_{0.95}Y_{0.05}O_3$ and $SrCe_{0.95}Yb_{0.05}O_3$ is within 50% of the concentration of the Y or Yb dopant. [39] Therefore, a 1 mm thick $SrZr_{0.95}Y_{0.05}O_3$ membrane with 1 cm^2 surface area is expected to be able to transport 0.1 ml/min of H_2 away from the CH_4 pyrolysis system. Compared to the usual CH_4 feed rates of 25 ml/min for our experiments, this is clearly not a significant rate of hydrogen removal. However, with a 10 μm thick membrane, removal rates are 10 ml of hydrogen per minute, which will greatly affect CH_4 pyrolysis equilibrium even in flow systems.

Our experimental program to develop a $SrZr_{0.95}Y_{0.05}O_3$ membrane concentrates on creating oxide powders which readily sinter to form dense films. We currently use the glycine-nitrate process (GNP) [12] for this purpose. In GNP synthesis, the appropriate stoichiometric ratio of metal nitrates ($ZrO(NO_3)_2$, $Sr(NO_3)_2$, $Y(NO_3)_3$, from Strem Chemicals, all >99.9% purity) are mixed with water and glycine in a 1000 ml beaker. The amount of metal added is enough to form 5-15 g of metal oxide. The metal nitrates and glycine are dissolved in approximately 50-100 ml of deionized H_2O and the glycine to nitrate molar ratio was 5:9. (5:9 is the stoichiometric ratio required to produce only CO_2, H_2O, and N_2 during combustion.) The beaker was placed on a hot plate on high heat, and covered loosely with a 100 mesh stainless steel wire screen. The screen prevents excessive powder loss during the reaction; one corner, however, must be left open to prevent pressurization of the beaker by rapid venting of evolved gases. When the homogeneous solution is heated slowly, water evaporates and the boiling temperature increases as the solution becomes more concentrated. After the solution becomes a thick slurry, it spontaneously reacts to form a light “ash” of small particles of mixed metal oxides. Local temperatures in these mixtures exceed 1100-1400°C, depending on the metal oxide being formed, because of the combustion of the glycine and nitrate “fuel”.

The resulting powder is examined by thermogravimetric analysis (TGA) using a DuPont Instruments 951 Thermogravimetric Analyzer and Dupont analysis software. A heating rate of 10°C/min was used in air flowing at 80 ml/min in order to record weight changes caused by burn-off of excess glycine, ash, and small amounts of metal nitrates and $SrCO_3$ remaining after GNP synthesis.

With this powder, we have prepared thick films (~1 mm thickness) by pressing the $SrZr_{0.95}Y_{0.05}O_3$ powder into a 19.05 or 25.4 mm diameter steel die at ~200 MPa in a uniaxial press. These "green" discs are then packed loosely with $SrZr_{0.95}Y_{0.05}O_3$ powder into an Al_2O_3 crucible and sintered at 1600°C for 4 hours in flowing air (99.999% pure). The disc's bulk density is calculated by suspending the disc in water and weighing the change of weight of the water bath to get the disc volume (Archimedes' method). The disc dimensions are measured with a micro-caliper to confirm the volume measurement. The theoretical density is calculated from literature crystal structure data.

The purpose of the thick membranes is to study the sintering properties of the $SrZr_{0.95}Y_{0.05}O_3$ powder and prepare membranes for use in H-transport experiments in a recirculating reactor. As shown previously, these discs do not have adequate hydrogen flux to improve the performance of CH_4 pyrolysis in a flow system. We therefore also use spin-coating methods to deposit the oxide powder as thin films on porous ceramic substrates.

5. Results

5.1 Computer simulations

The reduced reaction network for homogeneous CH_4 pyrolysis discussed above was tested for accuracy by comparison to the experimental results of Chen, et al. [40] Figure 2 compares the computer model with experimental results for homogeneous CH_4 pyrolysis in a batch reactor at 765°C. The agreement is excellent; however, the predicted (and experimental) methane conversions are very low (<1%) at these temperatures.

In methane pyrolysis, the primary reaction pathways are recombination and addition reactions involving methyl radicals. Therefore, any species that increases the rate of methyl radical generation will increase the yield of C_{2+} products. The initiation reaction can be generalized as

$$CH_4 + R \xrightarrow{k_i} CH_3 \cdot + RH \tag{4}$$

where R is any species which serves as a methyl radical generator by abstracting an H-atom from methane. Dean [16] demonstrated that the well-known "auto-catalysis" of methane is caused by the generation of high molecular weight species which act as homogeneous catalysts ("R" in equation 4) for methyl and hydrogen radical production. Hydrogen radicals, in turn, are the most reactive radical species and further accelerate the

generation of methyl radicals by forming H_2 from CH_4. The rapid increase in product yield, seen after 30 minutes in Figure 2, is a result of this increase in methyl radical concentration.

Figure 2: Experimental results [40] vs. simulation for CH_4 pyrolysis.
(765°C, 58.8 kPa, batch reactor)

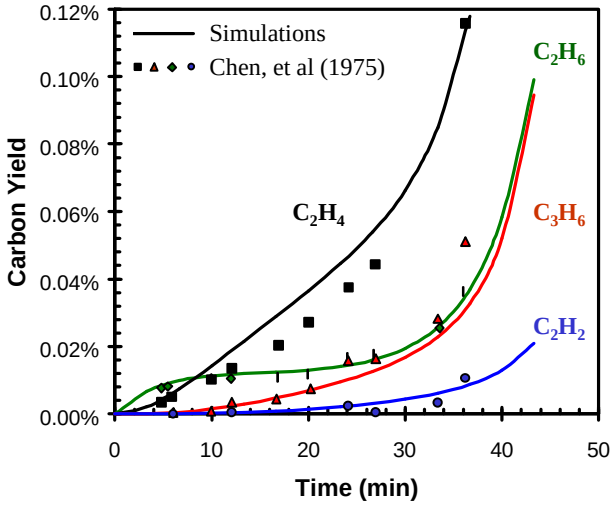

The methyl radical generator "R" in equation 4 can be provided by a surface active site. The results of adding this reaction (see equations 1 and 2) are shown in Figure 3. The major effect of surface-catalyzed methyl radical generation is an increase in the rate of methane conversion; the product selectivity is only slightly affected. Figure 3 also shows the intermediate nature of the desired C_2-C_{10} products in methane pyrolysis. C_2-C_5 species (especially ethane, ethylene, and propylene) are initial products, which are converted to thermodynamically stable aromatic species, especially benzene and naphthalene, as CH_4 conversion increases. These products are favored over the growth of linear or highly-branched paraffin and olefin species due to the stability of aromatic rings. Ultimately, however, the yield of these one- and two-ring aromatic species decreases as multi-ring polynuclear aromatic species (C_{11+}) dominate the product distribution above 23% CH_4 conversion, which is the equilibrium conversion when only C_2-C_{10} products are formed. Thus, the sequential nature of CH_4 pyrolysis can be roughly summarized as the following:

$$CH_4 \rightarrow \{C_2 - C_3\} + H_2 \rightarrow \{C_6 - C_{10}\} + H_2 \rightarrow \{C_{11+}\} + H_2 \qquad (5)$$

The results shown in Figure 3 demonstrate that the maximum C_2-C_{10} product yield in methane pyrolysis below 800°C is about 14%, unless another catalytic function is added or one or more of the products are removed during reaction. We simulated the irreversible removal of hydrogen from the reaction system by adding equation 3 to the homogeneous-heterogeneous network used to generate Figure 3. This simulation represents the physical situation for the hydrogen-transport membrane reactor shown in Figure 1. The effect of hydrogen removal on the C_2-C_{10} product yield is shown in Figure

Figure 3: Effect of surface-initiated CH_4 activation on predicted product yield.
(765°C, 58.8 kPa, batch reactor)

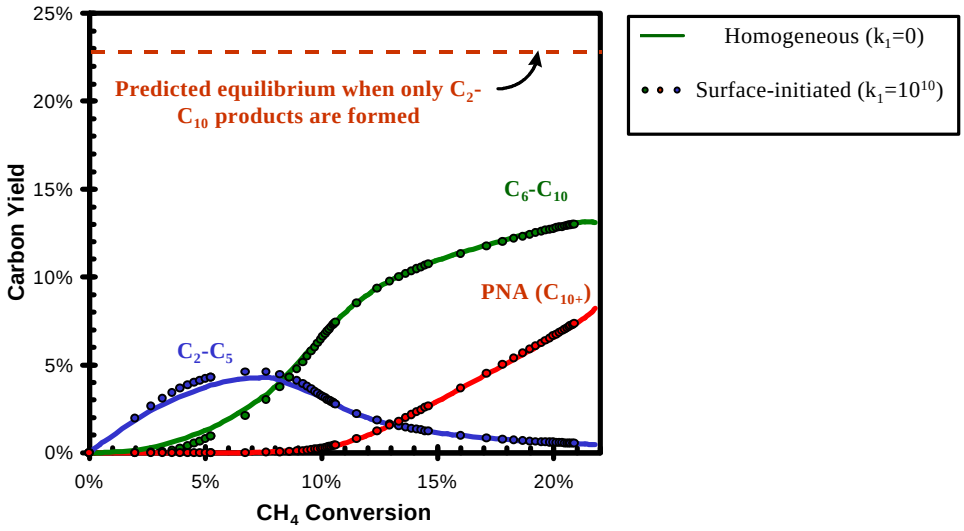

4. The rate of hydrogen removal in this case corresponds to Fickian diffusion through a 1 mm thick $SrZr_{0.95}Y_{0.05}O_3$ membrane at 700-800°C. The maximum C_2-C_{10} yield increases from 14% without hydrogen removal to nearly 42%. Very high methane conversion can be achieved because the thermodynamic limitation has been circumvented by hydrogen removal, but at the expense of C_2-C_{10} selectivity. The maximum yield occurs at 90% conversion, meaning that over half of the converted CH_4 goes to undesired polynuclear aromatic species. The reason for this loss of selectivity can be seen in equation 5; removal of hydrogen encourages C_{11+} formation as much as it does C_2-C_{10} formation.

Figure 4: Effect of hydrogen removal on predicted product yield.
(765°C, 58.8 kPa, batch reactor)

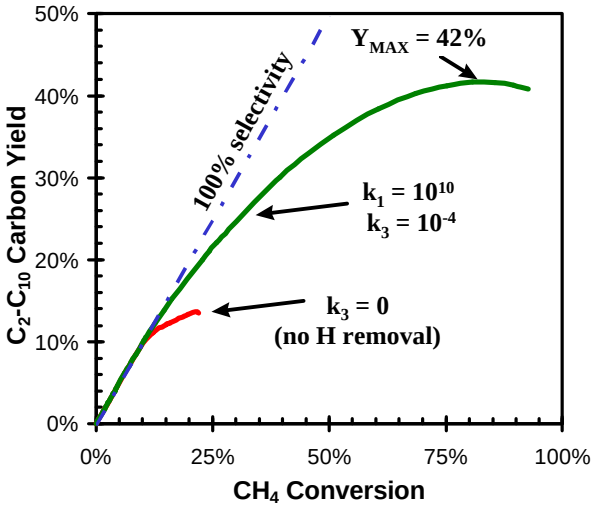

As shown before, the desired C_2-C_{10} species are intermediate products in CH_4 pyrolysis. Therefore we expect to be able to maximize the yield of these products by removing hydrogen at a rate significantly faster than the rate of polynuclear aromatic generation, effectively "trapping" the intermediate products. Figure 5 shows the effect of increasing the rate of hydrogen removal on the maximum yield of desired C_2-C_{10} products. Since the most straightforward method to increase the hydrogen removal rate is to decrease the thickness of the H-transport membrane, the x-axis of this graph can be considered to represent $SrZr_{0.95}Y_{0.05}O_3$ membranes from 1 to 0.001 mm thickness. This simulation predicts a maximum C_2-C_{10} yield of approximately 85% with hydrogen removal through a 10 μm thick membrane. This is a significant improvement compared to the thermodynamic limit of 23% and the homogeneous kinetic limit of 14% achieved without hydrogen removal. Further increases in the hydrogen removal rate become counterproductive, because hydrogen removal favors polynuclear aromatic formation at higher CH_4 conversions. (see Figure 5)

Figure 5: Effect of rate of hydrogen removal on the maximum C_2-C_{10} yield.
(765°C, 58.8 kPa, batch reactor, $k_1=10^{10}cm^3/mol/s$)

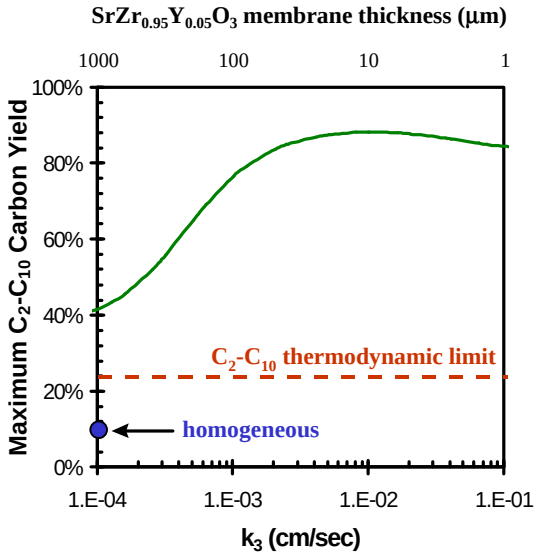

From these simulations, we can draw several conclusions about the methane pyrolysis system. Most importantly, C_2-C_{10} yield is limited by both thermodynamics and polynuclear aromatic chain growth. Surface-initiated CH_4 activation alone does not affect the product selectivity, therefore additional catalytic functions which act on the initial C_2-C_3 products are needed to catalytically control C_{11+} growth. C_{11+} formation can be controlled by using catalytic materials that inhibit chain growth, such as certain zeolites. H-ZSM5, for example, has a pore system too small to hold multi-ring aromatic species larger than naphthalene. In addition, the acid properties of H-ZSM5 prevent the formation of highly condensed coke species. [41] In conclusion, our simulations confirm that hydrogen removal from the system will influence favorably both the thermodynamics and kinetics of C_2-C_{10} formation during CH_4 pyrolysis. Thus, in contrast with methane

oxidative coupling, no intrinsic limitations prevent the attainment of high C_2-C_{10} product yields (~85%).

5.2 Catalytic methane pyrolysis

From the above simulations and the practical limits of $SrZr_{0.95}Y_{0.05}O_3$ materials, we conclude that CH_4 pyrolysis catalysts for use in our membrane reactor should:

1) catalytically activate CH_4 below 900°C
2) limit chain growth leading to PNA and coke formation
3) achieve reaction conditions in which hydrogen removal increases the yield of C_2-C_{10} products more than it does for C_{11+} condensed species
4) remain stable at reaction conditions or be easily regenerable
5) not be inhibited by ~3 kPa H_2O in the CH_4 mixture

Items 1 and 5 arise from the performance requirements for $SrZr_{0.95}Y_{0.05}O_3$ membranes as discussed in section 4.3. From several literature reports [4-6, 9], and our own work, Mo/H-ZSM5 catalysts seem to satisfy the above criteria. This section contains the results of our studies on the catalytic behavior of this system.

Figure 6 shows the results of methane pyrolysis on 2 wt% Mo/H-ZSM5 at 700°C. Before reaction, the catalyst was heated at a rate of 10°C per minute to the reaction temperature and held there for 30 minutes in a flowing air stream (100 ml/min of 20% O_2 in He). The reactor was flushed with helium for ten minutes, then a CH_4/Ar (1:1) mixture was introduced at a flow rate of 25 ml/min. During an initial activation period, lasting approximately 2-4 hours, CH_4 conversion was high and the major product was some type of solid carbonaceous species deposited on the catalyst. CO and H_2O were also formed during this period, showing that the MoO_3 species, present after the air pre-treatment, reduce under methane at 700°C. The solid carbon deposited during this period is likely a combination of olefinic and aromatic surface species [41], molybdenum carbide (~ Mo_2C) [6, 9], and carbidic species associated with the formation of Mo_2C. Such excess carbidic species are known to form on Mo_2C in pure CH_4 feed streams.

After 4 hours on stream, CO and H_2O formation decrease to nearly zero and carbon formation becomes less than 20% of the total product distribution. (The percent selectivity values reported are based on carbon selectivity, not molar.) Benzene (~60%), toluene (~10%), ethylene (~5-20%), and naphthalene (~5-10%) are the major gaseous products at steady-state. Ethane and propane are also measured in trace amounts. CH_4 conversion decreases slowly to approximately 4% after 16 hours reaction time. This deactivation is likely caused by a buildup of carbonaceous species within the ZSM5 pores and carbidic species around the Mo_2C particles. This carbon build-up causes pore-plugging and a loss of surface area and acid sites. [4] The catalytic activity can be recovered by cooling the catalyst to 100°C in helium, then heating at 5°C/min to 700°C in flowing air. Our studies have shown that rapid burning of the carbonaceous deposits by using a high heating rate (20°C/min) or by introducing air directly at the reaction

temperature leads to the destruction of the H-ZSM5 crystal structure (measured by XRD). This amorphous-zeolitic structure is almost completely inactive for CH_4 conversion (<1%) after three "rapid" regenerations.

Figure 6: CH_4 pyrolysis on 2 wt% Mo/H-ZSM5 at 700°C.

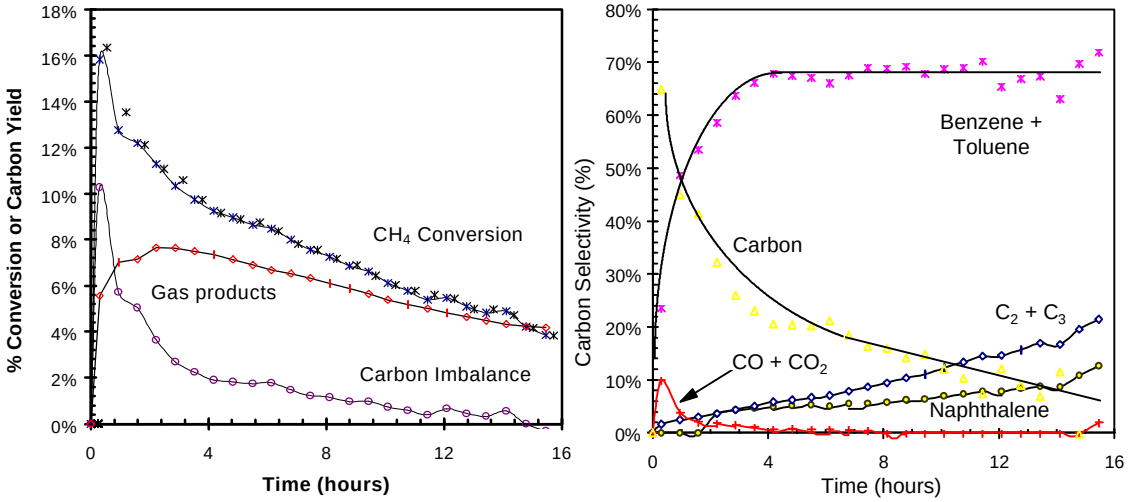

{Pretreatment: 100 ml/min (20% O_2 in He), 10°C/min to 700°C (30 min)}
{Reaction: 1.0 g 2 wt% Mo/H-ZSM5, 25 ml/min CH_4/Ar (1:1)}

Based on these results and other reports of CH_4 pyrolysis on Mo/H-ZSM5 [4-6, 9] and alkane activation on Ga, Zn/H-ZSM5 [42], we can postulate the following general mechanism for this reaction:

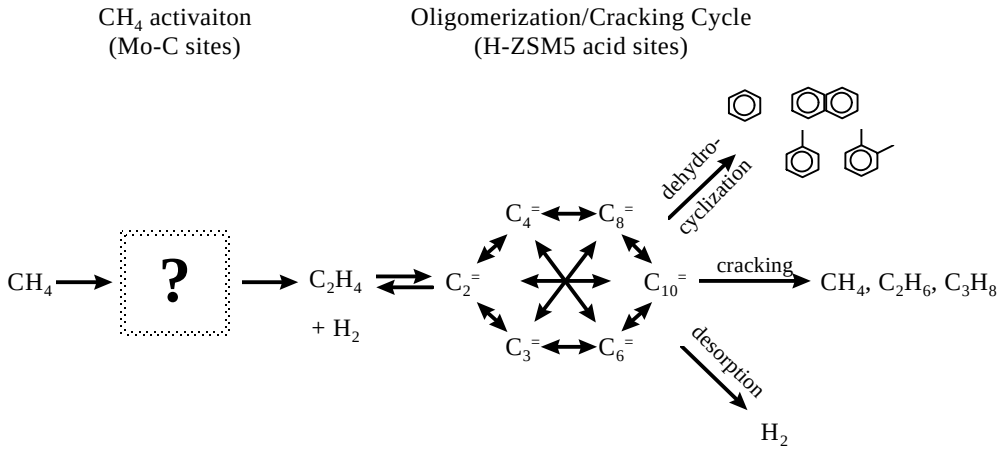

A large body of evidence exists indicating that ethylene is the primary intermediate product and reacts on the H-ZSM5 acid sites to give the final product distribution [4-6, 9]; the most convincing result is that C_2H_4 reaction on either Mo/H-ZSM5 or H-ZSM5 will give an almost identical product distribution as CH_4 on Mo/H-ZSM5. [9] The details of the first step, methane activation and formation of ethylene, are not well-understood and will be explored in the rest of this section.

We conducted temperature-programmed reduction on the fresh Mo/H-ZSM5 catalyst in order to examine the reduction of MoO_3 species during initial activation in CH_4 pyrolysis. Figure 7 shows the results of this experiment, and of a TPR of bulk MoO_3. Three distinct peaks, at 530, 670, and 1015°C, are visible in the reduction of fresh (fully oxidized) 2 wt% Mo/H-ZSM5. The peak at 530° is not as defined as the other two, and we attribute it to an amorphous, non-uniform distribution of poly-molybdate crystallites. This species would not appear as MoO_3 in X-ray diffraction patterns, and has been previously detected in TPR spectra of SiO_2- and Al_2O_3-supported MoO_3. [31] At this temperature, the reduction mechanism is autocatalytic; after a Mo site is reduced, the resulting exposed metal atom catalyzes the dissociation of hydrogen and rapidly reduces all remaining MoO_3 within range of surface hydrogen migration. The peak at 1015° has been attributed [31] to isolated MoO_2 species, which cannot undergo the low-temperature, autocatalytic reduction mechanism. Since the peak at 1015° must have a lower-temperature peak corresponding to isolated MoO_3 → MoO_2, we assign the peak at 670° to this initial reduction. By separating the 670° peak from the 530° peak as shown in Figure 7, the area of the former becomes about one-half of the area of the high-temperature peak at 1015°. We therefore believe the peak at 530°C to be caused by the complete reduction of poly-MoO_3 species, likely located on the outside of the H-ZSM5 crystallites since the pore channels are too small to not be blocked by such species. The peaks at 670° and 1015°C reflects isolated MoO_3 species which undergo a two-step reduction, Mo^{6+} → Mo^{4+} at 670°C and Mo^{4+} → Mo^0 at 1015°C. These isolated MoO_3 species are likely to reside at cation exchange sites in H-ZSM5, where they would be expected to exist as isolated cations, such as $(MoO_2OH)^+$ or bridging $(Mo_2O_5)^{2+}$ species.

Figure 7: TPR of 2 wt% Mo/H-ZSM5 and bulk MoO_3.

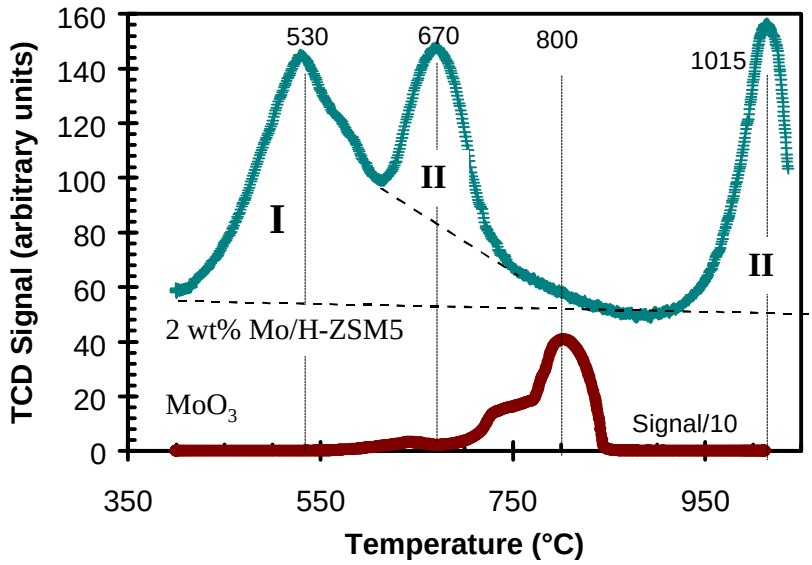

{TPR: 2 mg Mo in sample, heating rate 10°C/min, 80 ml/min H_2(20% in Ar)}

From the TPR results, we expect type I (poly-molybdate) Mo species to be fully reduced and type II (isolated molybdate) Mo species to be reduced to Mo^{4+} at 700°C under the reducing conditions of CH_4 pyrolysis. We also expect that type I reduced Mo species form molybdenum carbide in the presence of CH_4 at 700°C. Other groups have confirmed the presence of Mo_2C under these reaction conditions, using X-ray photoelectron spectroscopy (XPS). [6, 9] However, XPS has a limited probe depth, and will only detect species within a few unit cells from the outer surface of H-ZSM5 crystallites. The appearance of Mo_2C on the outer surface of H-ZSM5 crystallites agrees with our earlier speculation that the type I poly-molybdate species are located outside of the H-ZSM5 framework, and reduce to form Mo_2C under reaction conditions. Also, partially reduced (type II) species do not appear as Mo^{4+} in the XPS results, as expected from species located deep within zeolite crystallites.

Wang, et al., and Solymosi, et al., have shown that bulk and supported Mo_2C are inactive to CH_4 conversion at 700°C. [6, 9] We therefore speculated that active sites for CH_4 pyrolysis consist of isolated Mo^{4+} species of type II. In order to see if these partially reduced species were more active than the original MoO_3 species in the fresh catalyst, we conducted a series of temperature-programmed surface reactions (TPSR) on Mo/H-ZSM5. Figure 8 shows the results of the first of these experiments, air pretreatment of fresh 2 wt% Mo/H-ZSM5 followed by slow (2.5°C/min) heating in flowing CH_4 to 700°C, where the catalyst was held for 30 minutes. The initial activation of CH_4 occurred at approximately 660°C, where MoO_3 species reduced and carburized and pyrolysis products began to appear.

Figure 8: Temperature-programmed surface reaction of CH_4 pyrolysis on 2 wt% Mo/H-ZSM5.

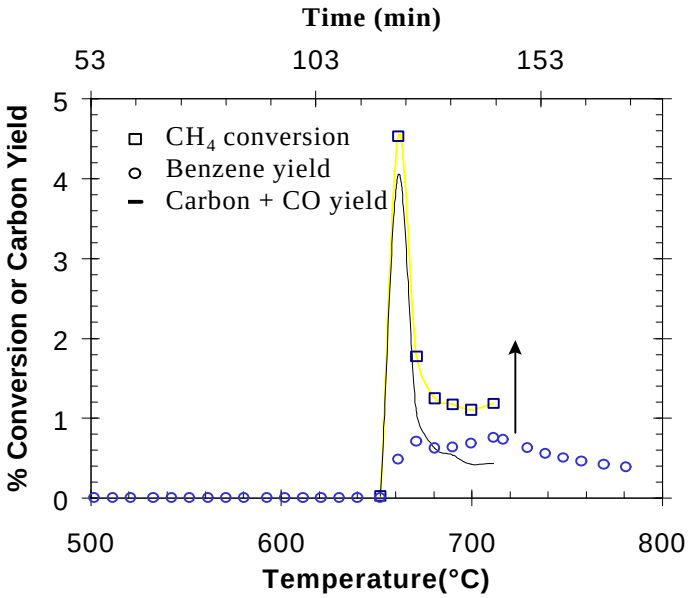

{Pretreatment: 100 ml/min (20% O_2 in He), 5°C/min to 700°C (30 min), cool to 300°C}
{TPSR: 0.1 g 2 wt% Mo/H-ZSM5, heating rate 2.5°C/min to 700°C, hold for 30 min}

A series of TPSR experiments were conducted using different pre-treatments, flow rates, and gas compositions. Table 1 gives a summary of these results. In Table 1, the initial activation temperature is defined as the temperature at which pyrolysis products first appear. The percent deactivation at 700°C was calculated as the difference of hydrocarbon product yield at 700°C between the beginning and end of the final 30 minute hold period. In these experiments, the heated reactor volume was about 5 ml. Therefore, significant gas-phase reactions are expected to occur in the low-flow (10 ml/min) experiment. In the interpretation of this experiment, we take into account the possibility that initial products of homogeneous CH_4 pyrolysis (H_2, C_2H_6, and C_2H_4) exist in the gas stream that contacts the catalyst bed.

Table 1: Summary of TPSR results for different reactant compositions.

Pretreatment	CH_4/Ar (ml/min)	Additive (ml/min)	Helium (ml/min)	Initial Activation Temperature (°C)	% Deactivation at 700°C (30 min)
1) O_2	25	none	75	660	25
2) O_2	22	3 (H_2)	75	660	1
3) H_2	25	none	75	660	41
4) O_2	10	none	0	630	1
5) O_2	24	1 (C_3H_8)	75	610	86
6) O_2	24	1 (C_2H_4)	75	590	70

{Pretreatment: 100 ml/min (20% H_2 or O_2 in He), 5°C/min to 700°C (30 min), cool to 300°C}
{TPSR: 0.1 g 2 wt% Mo/H-ZSM5, heating rate 2.5°C/min to 700°C, hold for 30 min}

The main difference between the experiments listed in Table 1 is the presence of small quantities of C_{2+} hydrocarbons or H_2 in the reactant feed. With hydrogen pretreatment (run 3) or co-feed (runs 2 and 4), MoO_3 species are reduced well before the pyrolysis products appear. In these cases, no CO or H_2O was seen during the initial activation period, which occurred at the same temperature as the control experiment (run 1). This indicates that reduced Mo^0 or Mo^{4+} species are no more active for CH_4 pyrolysis than fully oxidized species. However, H_2 co-feed did have the effect of nearly eliminating the catalytic deactivation seen in CH_4 pyrolysis at 700°C. Li and Stair [41] demonstrated that the carbonaceous deposits formed on H-ZSM5 during propane pyrolysis at 500°C are mainly polyolefinic and aromatic species which are easily desorbed by helium purging. It is possible that the amount of H_2 present with the CH_4 feed in runs 2 and 4 hydrogenates these surface carbon species during the reaction, preventing deactivation caused by carbon build-up in the catalytic pores. This opens the possibility of regenerating the Mo/H-ZSM5 catalyst after CH_4 pyrolysis by *in situ* hydrogenation of the carbonaceous deposits at reaction temperature, eliminating the lengthy carbon burn process previously described.

When C_{2+} hydrocarbons were added to the CH_4 feed (or produced by homogeneous pyrolysis reactions before the catalyst bed in run 4), the reaction initiation temperature is significantly reduced. This indicates that sites for CH_4 activation consist of either Mo-carbide sites or surface carbocations. C_{2+} hydrocarbons are expected to readily form olefinic surface carbo-cations above 500°C, and also to carburize molybdenum

species more readily than CH_4. However, carbocation alone is not expected to activate methane, because CH_4 conversion in the presence of C_2-C_4 alkenes does not occur on H-ZSM5. [43]

In the above TPSR experiments, the C_{2+} feed is preferentially reacted on the Mo/H-ZSM5 catalyst, with C_{2+} conversion reaching ~40% in runs 5 and 6 and CH_4 conversion being very low, less than 0.5%. The product distribution produced by C_{2+} reactions includes significant amounts of C_2H_4, toluene, and o-xylene in addition to the benzene and naphthalene predominantly formed in CH_4 pyrolysis. We also observed a significant increase of the catalyst deactivation rate when C_{2+} is present in the feed. However, this deactivation was compensated in run 4 by the low amount of C_{2+} products and the higher concentration of H_2 also present in the feed mixture. Other groups have reported high CH_4 conversions on H-ZSM5 based catalysts when C_{2+} hydrocarbons were added to the feed stream. [43, 44] The experiments in these reports all operate near 100% conversion of the C_{2+} additive, so competition for active sites between the CH_4 and C_{2+} species is eliminated in downstream portions of the catalyst bed.

From our experiments, we conclude that the catalytic site for the initial activation of CH_4 is an isolated carburized Mo species. Therefore, a carbon source is required to form the active site, and C_{2+} additives serve this function at a lower temperature than CH_4 does. In fact, the initial activation of Mo/H-ZSM5 catalysts may not occur in pure CH_4, but requires a high temperature in order to form the initial products of pyrolysis, which then carburize Mo and form the site active for CH_4 conversion. Furthermore, this isolated Mo species is probably only reduced to Mo^{4+}, and therefore is more accurately termed an isolated Mo-oxy-carbide species.

5.3 Hydrogen-transport films

The GNP synthesis method produced a light foam of a light pink powder ($SrZr_{0.95}Y_{0.05}O_3$) and black ash. The foam was crushed easily, and the XRD pattern of the powder showed peaks for the $SrZrO_3$ perovskite phase, but with less crystallinity than powders prepared by a conventional high-temperature 1400°C calcination procedure, possibly as a result of smaller crystallites in the GNP sample. Peaks for $SrCO_3$ and ZrO_2 phases also appear in the XRD pattern, indicating that perovskite formation was incomplete during GNP synthesis. TGA of this powder showed significant weight loss up to 950°C, likely from CO_2 evolution from the glycine ash and $SrCO_3$. The GNP powder was therefore calcined at 950°C, the minimum temperature for complete oxide formation. Higher temperatures result in lower surface area powders that densify less readily.

Hydrogen conducting disks with $SrZr_{0.95}Y_{0.05}O_3$ composition and >95% of theoretical density were prepared by pressing the calcined powder into 19 mm diameter discs of approximately one gram mass and one millimeter thickness and then sintering the discs at 1600°C. Also, spin-coating methods are being used to deposit these oxides as thin films on porous ceramic substrates. After a final sintering step, dense films with thickness of about 0.01 mm can be prepared. [45]

6. Application

The combination of a selective CH_4 pyrolysis catalyst (Mo/H-ZSM5) and high-temperature hydrogen-transport membrane ($SrZr_{0.95}Y_{0.05}O_3$) can solve many of the technological obstacles in the selective conversion of methane to useful products. The formation of carbon oxides, which plagues oxidative coupling routes, is eliminated, while maintaining the exothermicity and favorable thermodynamics of that reaction. In addition, air can be used as the oxidant, because the methane feed is not diluted with the oxidant in the membrane reactor. Many oxidative coupling of methane proposals include an expensive oxygen separation plant in order to prevent the dilution of the product gas with large volumes of N_2. [46]

Other groups have proposed the use of hydrogen-selective transport membranes to couple these reactions in an electrochemical cell. [47-49] These efforts are restricted by the necessity of a metal electrode at the anode (methane side of the membrane), which rapidly forms coke on its surface at high temperatures. Similarly, palladium alloys have been employed as either a hydrogen transport membrane or hydrogen acceptor species in order to shift the equilibrium of CH_4 conversion to higher yields. [50] However, Pd alloys and other hydrogen-transport metals, like the Pt and Pd electrodes used in the electrochemical cells, readily form coke on their surfaces in the presence of CH_4 at high temperatures. Because surface carbon limits the yield of C_2-C_{10} products in CH_4 conversion with hydrogen removal, any species that accelerate coke formation must be eliminated.

Recently, Choudhary, et al. reported the conversion of CH_4 to aromatics in the presence of C_{2+} hydrocarbons at 400-600°C on H-galloaluminosilicate ZSM5 catalyst. [43] The best results were achieved with a mixture of iso-butene and CH_4 (molar ratio=0.5) at 500°C, with 100% conversion of iso-butene, 44% conversion of CH_4, and 94% selectivity to aromatics reported. The high CH_4 conversion in this case is possible because of the dilution of the CH_4 feed with higher hydrocarbons. Therefore, the H:C ratio of the total feed gas is 2.7, making this mixture thermodynamically equivalent to a pure CH_4 feed with 1.3 moles of H removed per mole CH_4. While these results are promising, the high value of alkenes make them unlikely to be financially attractive as large volume additives to natural gas in order to increase the conversion of CH_4. Light alkanes such as ethane and propane would be more likely candidates as additives in a practical system, but CH_4 conversions with alkane additives were much lower (12% with 0.7:1 mixture of propane:CH_4) than with alkenes. Coincidentally, natural gas at the well head often contains up to 10% C_{2+} alkanes. [46] The addition of even these small amounts to CH_4 has been shown to substantially increase the conversion of CH_4 on Mo/H-ZSM5 catalysts. [44]

Compared with existing and proposed CH_4 conversion technology, the membrane reactor design shown in Figure 1 will offer an attractive alternative after the initial proof of concept stage. The main inherent disadvantage of the design is that a substantial fraction of the hydrogen in the CH_4 feed has to be burned in order to drive the reaction to high

CH_4 conversion. It would be more desirable to release this fraction as H_2. However, a thermodynamic penalty must be paid for the reaction to achieve high yields, and the production of a large C_2-C_{10} fraction should be worth the price paid. Additionally, some hydrogen can be recovered as H_2, since the equilibrium of CH_4 conversion to C_2-C_{10} products remains favorable at 700°C with as much as 30 mole % H_2 in the product gas.

6. Future Activities

Our current efforts attack in parallel the issues of improved stability and performance of Mo/H-ZSM5 catalysts and of integrating the catalyst with the H-transport disks and films into a membrane reactor configuration. For the Mo/H-ZSM5 catalyst, our interests include the inhibitory effect of H_2 on carbon deposition, the increase in CH_4 conversion reported in the literature with C_{2+} addition at 400-600°C [43, 44], and the inhibition effect of H_2O briefly reported in the literature. [9] For the $SrZr_{0.95}Y_{0.05}O_3$ H-transport membrane, we are focusing on integrating the membrane with the catalyst to achieve simultaneous CH_4 conversion with hydrogen removal, and on preparing thinner membrane films to increase the hydrogen flux from the reaction system.

7. Acknowledgments

The authors acknowledge Lutgard De Jonghe, Steve Visco and Craig Jacobson of the Materials Sciences Division, Lawrence Berkeley National Laboratory for assistance with the preparation of ceramic membrane disks and films. We also acknowledge FETC and Rodney Malone for his technical stewardship of this project.

8. References

[1] G. E. Keller, Bhasin, M. M., "Synthesis of Ethylene via Oxidative Coupling of Methane. I. Determination of Active Catalysts," *J. Cat.*, **73** 9-19 (1982).

[2] A. L. Tonkovich, Carr, R. W., Aris, R., "Enhanced C_2 Yields from Methane Oxidative Coupling by Means of a Separative Chemical Reactor," *Science*, **262** 221-223 (1993).

[3] Y. Jiang, Yentekakis, I. V., Vayenas, C. G., "Methane to Ethylene with 85 Percent Yield in a Gas Recycle Electrocatalytic Reactor-Separator," *Science*, **264** 1563-1566 (1994).

[4] L. Chen, Lin, L., Xu, Z., Li, X., Zhang, T., "Dehydro-Oligomerization of Methane to Ethylene and Aromatics over Molybdenum/HZSM-5 Catalyst," *J. Cat.*, **157** 190-200 (1995).

[5] Y. Xu, Liu, S., Wang, L., Xie, M., Guo, X., "Methane Activation Without Using Oxidants Over Mo/HZSM-5 Catalyst," *Catal. Lett.*, **135** 135-149 (1995).

[6] F. Solymosi, Szoke, A., “Selective Oxidation of Methane to Benzene Over Molybdenum Catalysts,” presented at Symposium on Heterogeneous Hydrocarbon Oxidation, 211th National Meeting, American Chemical Society, New Orleans, LA, 1996.
[7] J. H. Lunsford, Rosynek, Michael P., Wang, Dingjun, “Non-Oxidative Conversion of Methane to Benzene over a Mo/ZSM-5 Catalyst,” presented at 4th International Natural Gas Symposium, Kruger National Park, South Africa, 1995.
[8] S. C. Reyes, Iglesia, E., Kelkar, C.P., "Kinetic-Transport Models of Bimodal Reaction Sequences - I. Homogeneous and Heterogeneous Pathways in Oxidative Coupling of Methane," *Chem. Engr. Sci.*, **48** 2643-2661 (1993).
[9] D. Wang, Jack H. Lunsford, Michael P. Rosynek, "Catalytic conversion of methane to benzene over Mo/ZSM-5," *Topics in Cat.*, **3** 289-297 (1996).
[10] S. Shin, Huang, H.H., Ishigame, M., Iwahara, H., "Protonic Conduction in the Single Crystals of $SrZrO_3$ and $SrCeO_3$ Doped with Y_2O_3," *Solid State Ionics*, **40/41** 910-913 (1990).
[11] T. Schober, Friedrich, J., and Condon, J.B., "Effective Hydrogen Diffusivity in $SrCe_{0.95}Yb_{0.05}O_{3-\alpha}$ and $SrZr_{0.95}Yb_{0.05}O_{3-\alpha}$," *Solid State Ionics*, **77** 175-179 (1995).
[12] L. A. Chick, Pederson, l.R., Maupin, G.D., Bates, J.L., Thomas, L.E., Exarhos, G.J., "Glycine-Nitrate Combustion Synthesis of Oxide Ceramic Powders," *Mater. Letters*, **10** 6-12 (1990).
[13] C. A. Mims, Mauti, R., Dean, A. M., Rose, K. D., "Radical Chemistry in Methane Oxidative Coupling: Tracing of Ethylene Secondary Reactions with Computer Models and Isotopes," *J. Phys. Chem.*, **98** 13357-13372 (1994).
[14] D. L. Baulch, "Evaluated Kinetic Data for Combustion Modeling Supplement I," *J. Phys. Chem. Ref. Data*, **23** 847 (1994).
[15] W. Tsang, "Chemical Kinetic Database for Hydrocarbon Pyrolysis," *Ind. Eng. Chem. Res.*, **31** 3 (1992).
[16] A. M. Dean, "Detailed Kinetic Modeling of Autocatalysis in Methane Pyrolysis," *J. Phys. Chem.*, **94** 1432 (1990).
[17] A. M. Dean, Bozzelli, J. W., Ritter, E. R., "CHEMACT: A Computer Code to Estimate Rate Constants for Chemically- Activated Reactions," *Combust. Sci. and Tech.*, **80** 63-85 (1991).
[18] A. M. Dean, "Predictions of Pressure and Temperature Effects upon Radical Addition and Recombination Reactions," *J. Phys. Chem.*, **89** 4600-4608 (1985).
[19] D. R. Stull, Edgar F. Westrum, Jr., Gerard C. Sinke, *The Chemical Thermodynamics of Organic Compounds*. Malabar, Florida: Robert E. Krieger Publishing Co., 1987.
[20] S. W. Benson, *Thermochemical Kinetics: Methods for the Estimation of Thermochemical Data and Rate Parameters*, 2 ed. New York: John Wiley and Sons, 1976.
[21] S. E. Stein, Fahr, A., "High-Temperature Stabilities of Hydrocarbons," *J. Phys. Chem.*, **89** 3714-3725 (1985).
[22] M. Frenklach, "On the Driving Force of PAH Production," *22nd Symp. (Int.) on Comb.* 1075-1082 (1988).

[23] L. M. Aparicio, Rossini, S. A. , Sanfilippo, D. G. , Rekoske, J. E. , Trevino, A. A. , Dumesic, J. A., "Microkinetic Analysis of Methane Dimerization Reaction," *Ind. Eng. Chem. Res.*, **30** 2114-2123 (1991).
[24] T. Ito, Lunsford, J. H., "Synthesis of ethylene and ethane by partial oxidation of methane over lithium-doped magnesium oxide," *Nature*, **314** 721-722 (1985).
[25] R. L. Burwell, "The Role of Surface-Generated Gas-Phase Radicals in Catalysis," *Chemtracts-Anal., Phys., and Inorg. Chem.*, **2** 58-60 (1990).
[26] H. Iwahara, Esaka, T., Uchida, H., Maeda, N., "Proton Conduction in Sintered Oxides and Its Application to Steam Electrolysis for Hydrogen Production," *Solid State Ionics*, **3/4** 359-363 (1981).
[27] R. J. Kee, Rupley, F.M., Miller, J.A.,, 7.3 ed. Sandia, NM: Sandia Report SAND89-8009, UC-401, 1990.
[28] A. E. Lutz, Kee, R. J., Miller, J. A.,, 1.8 ed. Livermore, CA: Sandia National Laboratories, Report SAND87-8248, UC-401, 1992.
[29] R. W. Borry, Enrique Iglesia, "Computer simulation of methane conversion with continuous hydrogen removal," *(in preparation)* (1997).
[30] D. R. Lide,, 71 ed. Boca Raton: CRC Press, Inc., 1990.
[31] J. R. Regalbuto, Ha, J-W, "A Corrected Procedure and Consistent Interpretation for Temperature Programmed Reduction of Supported MoO_3," *Catal. Lett.*, **29** 189-207 (1994).
[32] H. Iwahara, Esaka, T., Uchida, H., Maeda, N., "Proton Conduction in Sintered Oxides and Its Application to Steam Electrolysis for Hydrogen Production," *Solid State Ionics*, **3/4** 359-363 (1981).
[33] H. Iwahara, Yajima, T., Hibino, T., Ozaki, K., Suzuki, H., "Protonic Conduction in Calcium, Strontium, and Barium Zirconates," *Solid State ionics*, **61** 65-69 (1993).
[34] T. Yajima, Suzuki, H., Yogo, T., Iwahara, H., "Protonic Conduction in $SrZrO_3$-Based Oxides," *Solid State Ionics*, **51** 101-107 (1992).
[35] M. J. Scholten, Schoonman, J., van Miltenburg, J.C., Oonk, H.A.J., "Synthesis of Strontium and Barium Cerate and Their Reaction with Carbon Dioxide," *Solid State Ionics*, **61** 83-91 (1993).
[36] R. W. Borry, Enrique Iglesia, (unpublished results).
[37] H. Iwahara, Esaka, T., Uchida, H., Yamauchi, T., Ogaki, K., "High Temperature Type Protonic Conductor Based on $SrCeO_3$ and Its Application to the Extraction of Hydrogen Gas," *Solid State Ionics*, **18/19** 1003-1007 (1986).
[38] H. H. Huang, Ishigame, M., Shin, S,, "Protonic Conduction in the Single Crystals of Y-doped $SrZrO_3$," *Solid State Ionics*, **47** 251-255 (1991).
[39] F. Krug, Schober, T., Springer, T., "In situ Measurements of the Water Uptake in Yb doped $SrCeO_3$," *Solid State Ionics*, **81** 111-118 (1995).
[40] C.-J. Chen, Back, M.H., Back, R.A., "The Thermal Decomposition of Methane. I. Kinetics of the Primary Decomposition to C_2H_6 + H_2; Rate Constant for the Homogeneous Unimolecular Dissociation of Methane and Its Pressure Dependence," *Can. J. Chem.*, **53** 3580 (1975).
[41] C. Li, Peter C. Stair, "Ultraviolet Raman spectroscopy characterization of coke formation in zeolites," *Cat. Today*, **33** 353-360 (1997).

[42] J. A. Biscardi, Enrique Iglesia, "Structure and function of metal cations in light alkane reactions catalyzed by modified H-ZSM5," *Cat. Today*, **31** 207-231 (1996).
[43] V. R. Choudhary, Anil K. Kinage, Tushar V. Choudhary, "Low-temperature nonoxidative activation of methane over H-galloaluminosilicate (MFI) zeolite," *Science*, **275** 1286-1288 (1997).
[44] L. B. Pierella, Linsheng Wang, Oscar A. Anunziata, “Studies on the methane conversion to aromatic hydrocarbons over modified zeolites,” presented at Actas XIII Iberoamerican Congress on Catalysis, Buenos Aires, Argentina, 1996.
[45] C. Jacobson, Steve Visco, Lutgard De Jonghe,: Materials Sciences Division, Lawrence Berkeley National Laboratory, 1997.
[46] J. W. M. H. Geerts, J.H.B.J. Hoebink, K. van der Wiele, “Ethylene from natural gas: proven and new technologies,” in *Novel production for ethylene, light hydrocarbons and aromatics*, L. F. Albright, Billy L. Crynes, Siegfried Nowak, Ed. New York: Marcel Dekker, Inc., 1991.
[47] L. S. Woldman, Sokolovskii, V.D., "Electrocatalytic Methane Coupling in the Abscence of Oxygen on a High-Temperature Proton-Conducting Electrolyte," *Catal. Lett.*, **8** 61-66 (1991).
[48] S. Hamakawa, Hibino, T., Iwahara, H., "Electrochemical Methane Coupling Using Protonic Conductors," *J. Electrochem. Soc.*, **140** 459 (1993).
[49] P. H. Chiang, Eng, D., Alqahtany, H., Stoukides, M., "Nonoxidative Methane Coupling with the Aid of Solid Electrolytes," *Solid State Ionics*, **53-56** 135-141 (1992).
[50] A. Anderson, Ivar M. Dahl, Klaus-Joachim Jens, Erling Rytter, Ase Slagtern, Age Solbakken, "Hydrogen acceptor and membrane concepts for direct methane conversion," *Cat. Today*, **4** 389-397 (1989).